APSB

ORIGINAL ARTICLE

Synergistic activation of AMPK by AdipoR1/2 agonist and inhibitor of EDPs−EBP interaction recover NAFLD through enhancing mitochondrial function in mice

Nazi Song[a,†], Hongjiao Xu[a,†], Shuohan Wu[a,†], Suijia Luo[d], Jingyao Xu[a], Qian Zhao[a], Rui Wang[b,c,*], Xianxing Jiang[a,*]

[a]School of Pharmaceutical Sciences, Sun Yat-sen University, Guangzhou 511400, China
[b]State Key Laboratory of Bioactive Substance and Function of Natural Medicines, Institute of Materia Medica, Chinese Academy of Medical Sciences & Peking Union Medical College, Beijing 100050, China
[c]School of Life Sciences, Key Laboratory of Preclinical Study for New Drugs of Gansu Province, School of Basic Medical Sciences & Research Unit of Peptide Science, Lanzhou University, Lanzhou 730000, China
[d]Shenzhen Turier Biotech. Co., Ltd., Shenzhen 518118, China

Abstract Nonalcoholic fatty liver disease (NAFLD), especially nonalcoholic steatohepatitis (NASH), is a common hepatic manifestation of metabolic syndrome. However, there are no effective therapy to treat this devastating disease. Accumulating evidence suggests that the generation of elastin-derived peptides (EDPs) and the inhibition of adiponectin receptors (AdipoR)1/2 plays essential roles in hepatic lipid metabolism and liver fibrosis. We recently reported that the AdipoR1/2 dual agonist JT003 significantly degraded the extracellular matrix (ECM) and ameliorated liver fibrosis. However, the degradation of the ECM lead to the generation of EDPs, which could further alter liver homeostasis negatively. Thus, in this study, we successfully combined AdipoR1/2 agonist JT003 with V14, which acted as an inhibitor of EDPs−EBP interaction to overcome the defect of ECM degradation. We found that combination of JT003 and V14 possessed excellent synergistic benefits on ameliorating NASH and liver fibrosis than either alone since they compensate the shortage of each other. These effects are induced by the enhancement of the mitochondrial antioxidant capacity, mitophagy, and mitochondrial biogenesis *via* AMPK pathway. Furthermore, specific suppression of AMPK could block the effects of the combination of JT003 and V14 on reduced oxidative stress, increased mitophagy and

mitochondrial biogenesis. These positive results suggested that this administration of combination of AdipoR1/2 dual agonist and inhibitor of EDPs−EBP interaction can be recommended alternatively for an effective and promising therapeutic strategy for the treatment of NAFLD and NASH related fibrosis.

1. Introduction

Nonalcoholic fatty liver disease (NAFLD) is a progressive liver disease caused by excessive triglycerides (TG) accumulation in hepatocytes, mainly ranges from simple steatosis to hepatitis and progression to advanced fibrosis, cirrhosis and hepatocellular carcinoma[1,2]. At present, there are many different classes of NAFLD drugs which are underdevelopment, for example farnesoid X receptor agonists, thyroid hormone receptor agonists, fibroblast growth factor agonists, and peroxisome proliferator-activated receptor (PPAR) agonists[3,4]. Unfortunately, the clinical trials of these NAFLD candidates were far from satisfactory[5]. Genfit announced that elafibranor, a dual PPARα/δ agonist, failed to achieve significant improvement in non-alcoholic steatohepatitis (NASH) patients with stage 2 or 3 fibrosis[6]. Ocaliva, a farnesoid X receptor agonist, was recently rejected by the US Food and Drug Administration[7]. Therefore, it is urgent to develop new approaches for developing promising treatment strategies for NAFLD. Because the pathophysiology of NAFLD is complex, several targets and pathways must be tackled to improve the therapeutic efficacy of NAFLD treatments, more and more attention has been gained on the combination therapy[8].

Adiponectin, an adipocytokine, mainly produced by mature adipocytes[9], plays a pivotal role in cellular energy management[10,11], extracellular matrix (ECM) metabolism[12,13], proliferation[14,15], and migration[16,17]. Clinical studies had demonstrated that plasma adiponectin decreased in NAFLD individuals[18,19]. And accumulating evidence demonstrated that adiponectin receptors (AdipoRs) are potential drug targets for NAFLD therapy[20−22]. We reported previously that JT003 (P-Nva-LYYFA), an AdipoR1/2 dual agonist, attenuated liver fibrosis *via* amelioration of ECM metabolism and mitochondrial function[23]. However, it is not harmless to degrade ECM because the elastin, the main components of ECM in hepatic fibrosis nodules, undergoes a breakdown[24]. Elastin is abnormally synthesized and degraded in the diseased liver leading to the release of bioactive elastin-derived peptides (EDPs)[25,26]. It has been reported that plasma EDPs level are positively correlated with the degree of NAFLD. In addition, the accumulation of EDPs induces hepatic lipogenesis and fibrosis by the LKB1-adenosine monophosphate-activated protein kinase (AMPK) pathway followed by elastin receptor complex activation[27]. The V14 peptide (VVGSPSAQDEASPL), which correspond to part of the elastin binding protein sequence, can bind to the circulated EDPs and block their effects[28]. JT003 induces the production of EDPs, which in turn affect the therapeutic ability of JT003. And it will be a better strategy if the effect of EDPs was blocked during the treatment. What's more, synergistic drug combinations have many advantages over monotherapy for complex diseases, including reduced side effects, reduced drug resistance, and increased efficacy. These ad-

vantages are mainly due to the targeting of multiple molecular networks in the body[29]. Therefore, we hypothesize that a combination of JT003 and V14 is more effective than either alone for amelioration of NAFLD *in vitro* and *in vivo*.

To gain a better understanding of the scope of this conceptual combined therapeutic strategy and expand the traditional methodologies developing an efficient protocol for accessing potential candidates. In the current study, we identified a combination of AdipoR1/2 dual agonist and inhibitor of EDPs−EBP interaction as a positive synergistic therapeutic strategy to treat NAFLD in mice. We found that a combination of JT003 and V14 is more effective than either alone for the attenuation of lipid accumulation, hepatitis and liver fibrosis in mice by enhancing mitochondrial function and improving mitochondrial oxidative capacity *via* activation of AMPK pathways *in vitro* and *in vivo*. And the combination of AdipoR1/2 dual agonist and inhibitor of EDPs−EBP interaction has not been applied in NAFLD and will be a promising alternative therapeutic strategy.

2. Materials and methods

2.1. Human liver and serum samples

All procedures that involved human samples were approved by the First Affiliated Hospital of Sun Yat-sen University Review Board (Guangzhou, China) and were performed in a manner consistent with the principles outlined in the Declaration of Helsinki. Written informed consent was obtained from all study participants. Human serum samples were drawn after an overnight fast on the day of elective diagnostic liver biopsy procedure at the First Affiliated Hospital of Sun Yat-sen University. Control serum samples were collected form healthy female and male donors. Plasma was obtained by centrifugation of blood samples for 30 min at 3500 rpm at 4 °C and was immediately stored at −80 °C until further preparation. Human fibrotic liver biopsy was derived from patients undergoing liver transplant surgery who had been diagnosed as cirrhosis or hepatocellular carcinoma. Human non-fibrotic liver samples were collected from healthy regions of the livers from donors who had undergone liver resection because of a hepatocellular carcinoma or hepatic cyst. Patients with other liver diseases, including viral hepatitis, autoimmune hepatitis, primary biliary cirrhosis, hemochromatosis, drug-induced liver disease and other secondary hepatic diseases were excluded from this study. Human serum adiponectin levels were analyzed by enzyme linked immunosorbent assay (ELISA) kit for adiponectin (SEA605Hu). Human serum EDPs were measured by Fastin™ Elastin Assay (Biocolor, Carrickfergus, UK). In addition, the detailed information for the clinical characteristics of these samples is provided in Supporting Information Tables S1 and S2.

2.2. Animal models and tissue collection

Male C57BL/6J mice (7−8 weeks old) were purchased from Guangdong Medical Laboratory Animal Center and used to establish NASH and liver fibrosis models. The mice were housed in a standard environment with a 12 h day/night cycle and free to food and water. All animal protocols were approved by the Institutional Animal and Care Use Committee of the Sun Yat-sen University. The animals received humane care according to the criteria outlined in the Guide for the Care and Use of Laboratory Animals prepared by the National Academy of Sciences and published by the National Institutes of Health.

After 7 days of acclimatization, mice NASH and liver fibrosis models were established by methionine-choline deficient (MCD) or high fat diet (HFD) or carbon tetrachloride (CCl_4)[30,31]. In MCD-induced NASH model, mice were fed an MCD diet for 8 weeks (protein: 17%; carbohydrates: 66%; fat: 10%; MD12052, Medicience, Jiangsu, China). Mice administered a methionine-choline sufficient (MCS) diet serves as control group (protein: 17%; carbohydrates: 65%; fat: 10%; L-methionine: 0.3%; hydrochloride tartrate: 0.2%; MD12051, Medicience, Yangzhou, China). Then mice were randomly assigned into five groups according to different demands: MCS control group, MCD model group, MCD + JT003 group, MCD + V14 group, and MCD + JT003 + V14 group (n = 6 for each group).

In HFD-induced NASH model, mice were fed with an HFD diet (n = 6; protein: 18.1%; carbohydrates: 20.3%; fat: 61.6%; D12492, Research Diets, USA) or a regular chow diet (n = 6; protein: 18.3%; carbohydrates: 71.5%; fat: 10.2%; D12450B, Research Diets, USA) for 24 weeks. Then mice were randomly assigned into five groups according to different demands: Control group, HFD model group, HFD + JT003 group, HFD + V14 group, and HFD + JT003 + V14 group (n = 6 for each group).

In CCl_4-induced liver fibrosis model, mice were exposed to CCl_4 (dissolved 1:4 in corn oil) by intraperitoneally administered at a dose of 0.5 mL/kg twice a week for 6 weeks. The negative group mice were injected with corn oil (Aladdin, China) alone at the equivalent volume and frequency. Then mice were randomly assigned into five groups according to different demands: Oil group, CCl_4 model group, CCl_4+JT003 group, CCl_4+V14 group, and CCl_4+JT003 + V14 group (n = 6 for each group).

All peptides were synthesized and purified according to the standard method of solid-phase peptide synthesis and dissolved in PBS to prepare. JT003 (500 μg/kg/day) and V14 (150 μg/kg/3 days) were intraperitoneally (i.p.) administered in the last 4 weeks during HFD or MCD feeding and in the last 3 weeks during CCl_4 inducing damage. JT003 + V14 were administered separately according to the frequency and dose of the peptide itself.

At the end of the experiments, all mice above were need to overnight fast 8 h for further histological, biochemical, and mechanism studies. Blood was collected from the posterior orbital venous plexus of the eyes of ether anesthetized mice. Serum samples was obtained from centrifugation of blood at 3500 rpm for 15 min. Liver tissue was flash-frozen in liquid nitrogen prior to the store at −80 °C. The remaining tissue were fixed in 10% paraformaldehyde (Solarbio, Beijing, China) and prepared for subsequent pathological sections. The levels of aspartate aminotransferase (ALT), Aspartate transaminase (AST), TG, and superoxide dismutase (SOD) in serum were determined using commercial assay kits (Nanjing Jiancheng Bioengineering Institute, Nanjing, China).

2.3. Cell culture and treatment

The HepG2 (human hepatocellular liver carcinoma cell line) cell lines were purchased from the Type Culture Collection of the Chinese Academy of Sciences (Shanghai, China). The cells were cultured in Dulbecco's modified Eagle's medium (DMEM; Gibco) containing 10% fetal bovine serum (Gibco) and 1% penicillin/streptomycin (Gibco). For HepG2 cells, 0.25 mmol/L palmitic acid (PA) was administered to establish a cell model of lipid accumulation. The cells were randomly assigned into five groups according to different demands: bovine serum albumin (BSA), PA model group, PA + JT003 (200 μmol/L) group, PA + V14 (10 μmol/L) group, and PA + JT003 (200 μmol/L)+V14 (10 μmol/L) group (n = 3 for each group).

2.4. Primary cell isolation

Primary hepatocytes were acquired from 6- to 8-week-old female C57BL/6J mice using collagenase perfusion and gradient centrifugation[32]. In brief, the isolated cells were the filtered through a 70 μm cell strainer and were plated in collagen I-coated well plated in DMEM containing 10% fetal bovine serum and 1% penicillin−streptomycin. The cells were induced by 0.25 mmol/L PA and randomly assigned into five groups according to different demands: BSA, PA model group, PA + JT003 (200 μmol/L) group, PA + V14 (10 μmol/L) group, and PA + JT003 (200 μmol/L) + V14 (10 μmol/L) group (n = 5 for each group). PA or peptides were incubated with for 24 h. Then Oil Red O staining and cellular TG contents were performed to evaluate the accumulation of lipid droplets.

2.5. Histopathology assessment

The liver was embedded with tissue-Tek optimal cutting temperature compound (Sakura Finetek, Japan), or paraffin, and liver sections were prepared. Liver sections were used for H&E, Sirius Red, and Oil Red O staining (Servicebio, Wuhan, China). For immunohistochemistry, antigen retrieval was performed under high pressure and temperature in 0.01 mmol/L citrate buffer (pH = 6.0). Then, the sections were then incubated with 3% H_2O_2 at room temperature for 10 min to block the endogenous peroxidase activity. After blocked with 1% BSA, the sections were incubated with primary antibodies overnight at 4 °C and then secondary antibodies were used for 1 h at 37 °C. Immunochemical staining of collagen type I (Col1α), CD68, and 4 hydroxynonenal (4-HNE) was performed using paraffin-embedded liver sections. Detailed information about antibodies is listed in Supporting Information Table S3. Quantitative analysis was performed using open-source software (Image-J software (http://imagej.nib.gov/)).

2.6. CCK-8 viability assay

HepG2 cells were seeded in a 96-well plate with 7000 cells/well. Cell viability was detected by a Cell Counting Kit-8 (CCK-8, Beyotime Biotechnology, Shanghai, China) according to manufacturer's instructions. To assess the impact on cell viability, various concentrations of PA were added to the HepG2 cells for 24 h. After

incubation, the CCK-8 solution was added to the each well and incubated at 37 °C for 4 h. The absorbance was measured at 450 nm using a microplate reader. Cell viability was calculated by Eq. (1):

$$\text{Cell viability (\%)} = (\text{Experimental group absorbance value}/ \text{Control group absorbance value}) \times 100 \quad (1)$$

2.7. Quantitative real-time PCR analysis

Total RNA was extracted from primary hepatocytes, HepG2 cells, and tissue samples using TRIzol™ Reagent (Invitrogen, New York, USA). According to the TransStart® Top Green qPCR SuperMix (TransGen Biotech, Beijing, China), the extracted total RNA was reverse transcribed into cDNA for subsequent qPCR experiments. These primers were designed and synthesized by Sangon Biotech. And the sequences of the primers are listed in Supporting Information Tables S4 and S5. Glyceraldehyde-3-phosphate dehydrogenase (GAPDH) expression was used to normalize the mRNA expression levels of targets genes.

2.8. Western blot analysis

Primary hepatocytes, HepG2 cells, and liver samples were collected after treatment. It was lysed with RIPA buffer (Sigma−Aldrich, England) for 30 min and then centrifuged at $12,000 \times g$ for another 30 min. Mitochondrial protein was isolated using Mitochondria Isolation Kit (Beyotime Biotechnology, Shanghai, China). Protein concentration was measured using a Pierce™ BCA Protein Assay Kit (Thermo Fisher Scientific, New York, USA). The proteins were separated on an SDS-PAGE gel and transferred to a polyvinylidene fluoride membranes (Millipore, MA, USA). The membrane was blocked with 5% non-fat milk and the antibodies were incubated overnight at 4 °C. The next day, the membrane was washed in TBST and incubated with a secondary antibody, and the signal was chemiluminescence enhanced by Immobilon ECL Ultra Western HRP Substrate (Millipore, MA, USA). Detailed information about antibodies is listed in Table S3.

2.9. Mitochondrial DNA (mtDNA) quantification

Total DNA was extracted from liver tissues or primary hepatocytes using Mitochondrial DNA Isolation Kit (BioVision, USA). The mtDNA copy number was analyzed by normalizing the mitochondrial-encoded gene mitochondrially encoded cytochrome c (mtCol) to the nuclear-encoded gene NADH dehydrogenase flavoprotein 1 (Ndufv1) by qPCR using SYBR. Detailed information about primer sequence is listed in Table S4.

2.10. Flow cytometry

Primary hepatocytes were seeded in 6-well plate and incubated with Ad-GFP-LC3B (30 MOI) at 37 °C for 24 h. After incubation, the primary hepatocytes were washed with PBS and the cells were treated with or without 25 μmol/L chloroquine (CQ; Sigma−Aldrich, UK) for 6 h. Primary hepatocytes were harvested and washed with either immunostaining permeabilization solution with saponin (Beyotime Biotechnology, Shanghai, China) or PBS alone. After three times washing, the cells were detected with a CytoFLEX S Flow cytometer (Beckman, CA, USA) and analyzed using FlowJo software.

2.11. Agilent seahorse XF Cell Mito Stress test

The mitochondrial oxygen consumption rate (OCR) was measured using the Seahorse XFe96 analyzer (Agilent Technologies, CA, USA). Primary hepatocyte and HepG2 cells were seeded into a 96-well cell culture plate, and the cells were treated with drugs after adherence. The cell medium was replaced with a test solution (DMEM containing 5 mmol/L glucose, 4 mmol/L L-glutamine, 2 mmol/L sodium pyruvate, pH = 7.4) and the plate was placed in a 37 °C CO_2-free incubator for 1 h. The different mitochondrial inhibitors were used in the Seahorse XF Cell Mito Stress test kit (Agilent Technologies), including 1 μmol/L oligomycin, 1 μmol/L FCCP, and 0.5 μmol/L rotenone/antimycin A. Basal and maximal OCR were normalized with the mitochondrial protein concentration.

2.12. Cell confocal imaging

Mitochondrial superoxide was detected using MitoSOX Red Mitochondrial Superoxide Indicator (Yeasen, Shanghai, China), a mitochondrial superoxide indicator. Primary hepatocyte and HepG2 cells were seeded into a laser confocal Petri dish, adhered with drugs for 24 h, then cells were stained with 1 μmol/L MitoSOX for 20 min in the dark at 37 °C and counterstained with Hoechst33258 (Sigma−Aldrich, UK).

Mitochondrial membrane potential assay kit with JC-1 (Beyotime Biotechnology, Shanghai, China) was used to measure mitochondrial membrane potential. PA-induced primary hepatocytes and PA-induced HepG2 cells were washed with PBS and incubated with JC-1 buffer supplied by the JC-1 kit.

Cell mitochondria were co-stained with 200 nmol/L Mito-Tracker™ Green FM or 50 nmol/L Lyso-Tracker Red and Ad-GFP-LC3B (30 MOI; Beyotime Biotechnology, Shanghai, China). In short, primary hepatocytes and HepG2 cells were seeded in a laser confocal dish and infected with Ad-GFP-LC3B for 24 h. Then cells were incubated with according to drugs. Finally, the cells were as washed with PBS and incubated with MitoTracker™ Green FM. For mitochondrial and lysosomal colocalization, the cells were incubated for 1 h with MitoTracker™ Green FM and then added Lyso-Tracker Red for staining.

2.13. AMPK inhibition measurement

To verify the specificity of combination of JT003 and V14 in AMPK activation, we tested the effects of the AMPK inhibitor compound C (Selleck.cn, TX, USA). Cells were seeded into a 6-well plate and treated with 20 μmol/L compound C after cell adherence. After 3 h, cells were subjected to JT003 (200 μmol/L), V14 (10 μmol/L), and PA (0.25 mol/L) cotreatment for 24 h. After that, the cells were obtained for different experiments.

2.14. Statistical analysis

All positive area of staining was quantified by ImageJ (https://imagej.nih.gov/ij/). For graphs, all data are represented as mean ± standard error of mean (SEM) using Dunnett's test as the post hoc test following the one-way ANOVA or Tukey's test as the post hoc test following the two-way ANOVA. $^{\#}P < 0.05$, $^{\#\#}P < 0.01$ versus the control group; $^{*}P < 0.05$, and $^{**}P < 0.01$ versus the model group.

2.15. Data availability

All relevant data are available from the corresponding author upon reasonable request. All the data supporting the findings of this study are available within this article, supplementary information files, and Source Data file (https://doi.org/10.6084/m9.figshare.20494719). RNA-sequencing data that support the findings of this study have been deposited in the Sequence Read Archive under accession code SRR17305899 and SRR18385098. Source data are provided with this paper.
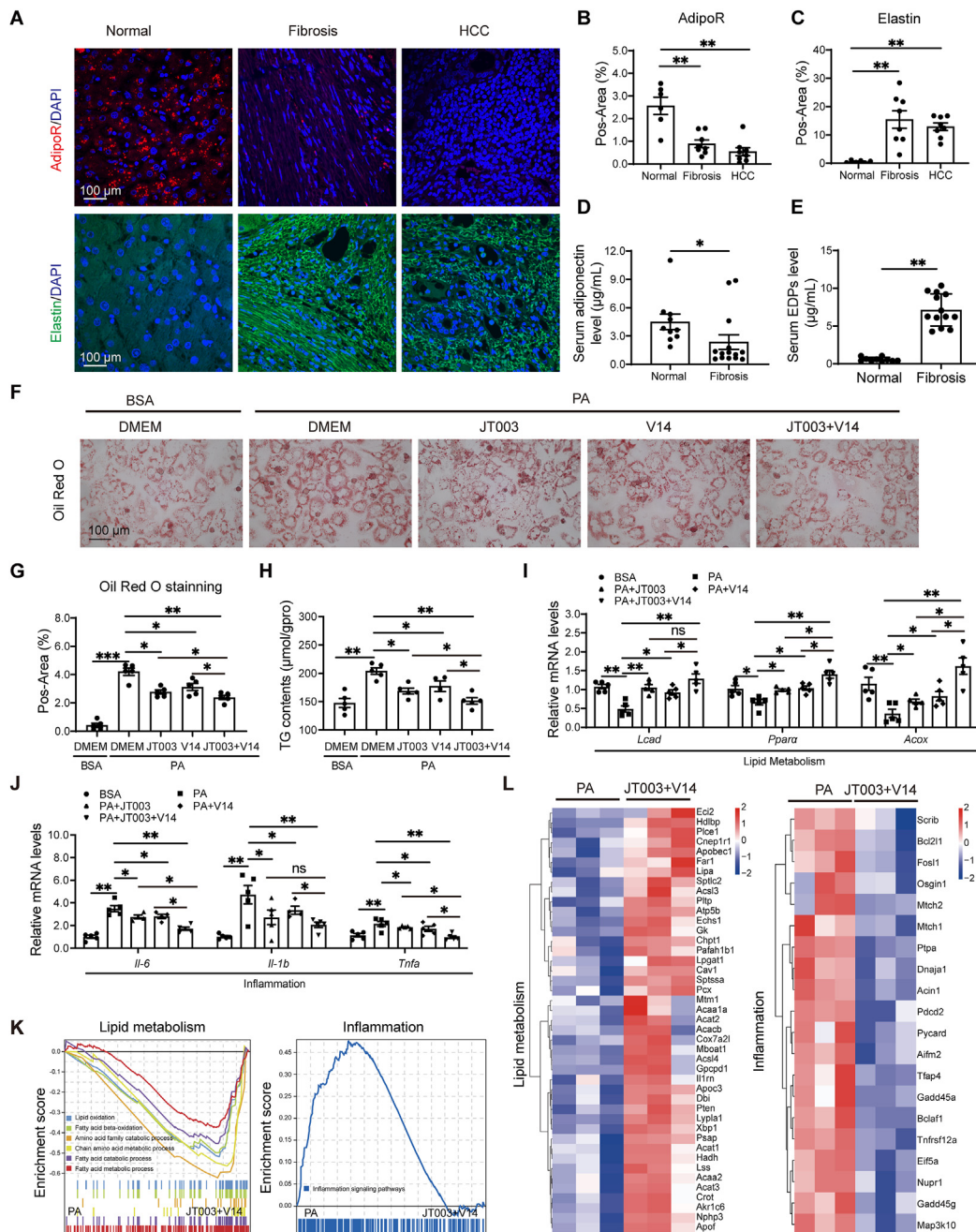
Figure 1 Histology and serum analysis in human samples along with JT003 + V14 attenuates lipid metabolism, and inflammation in hepatocytes. (A–C) Representative images showing immunohistochemistry (IHC) staining of AdipoR and elastin as well as image analysis of the positive area in formalin-fixed paraffin-embedding (FFPE) sections from non-fibrotic donors and from individuals with liver fibrosis ($n = 8$). (D, E) The levels of adiponectin and serum elastin-derived peptides (EDPs) were measured in human serum sample from non-fibrotic donors and from individuals with liver fibrosis ($n = 14$). (F, G) Representative Oil Red O staining in primary hepatocytes treated with palmitic acid (PA) or PA + JT003 + V14 ($n = 5$). (H) Analysis of triglyceride (TG) contents in the primary hepatocytes ($n = 5$). (I, J) mRNA levels of lipid metabolism and inflammation in primary hepatocytes treated with PA or PA + JT003 + V14 ($n = 5$). (K) GSEA pathways were analyzed in primary hepatocytes treated with PA or JT003 + V14 ($n = 3$). (L) Genes associated to lipid metabolism and inflammation in microarray analysis. For graphs, all data are represented as mean ± SEM using Dunnett's test as the *post hoc* test following the one-way ANOVA or Tukey's test as the *post hoc* test following the two-way ANOVA. *$P < 0.05$, **$P < 0.01$, ***$P < 0.001$, ns represents no significance.

3. Results

3.1. JT003 + V14 attenuates lipid metabolism and inflammation in PA-induced hepatocytes

To detect the potential trends of adiponectin and EDPs levels in liver fibrosis, we first analyzed 14 Chinese patients with liver fibrosis and 10 healthy volunteers, using immunohistochemistry (IHC), ELISA or Fastin™ Elastin Assay, respectively. Compared with healthy volunteers, the levels of AdipoR in hepatic sections and serum adiponectin were significantly decreased in patients with liver fibrosis, while the expression of elastin or serum EDPs were increased (Fig. 1A−E). These data verified the changing trends of adiponectin and EDPs in the fibrosis, and also provided a reliable basis for the combination of AdipoR1/2 dual agonist and antagonist of the EDPs receptor[18,33].

In order to investigate the effect of JT003 + V14 on inflammation and lipid accumulation in hepatocytes, primary hepatocytes and HepG2 cells were treated in presence of PA stimulation for 24 h. We first performed the CCK-8 kit to detect the viability of hepatocytes induced by various concentrations of PA. The result shows that an average of 20% cell viability decreased after treatment with PA in the range of concentration from 0.1 to 0.5 mmol/L was observed and the highest concentration of PA caused a 50% reduction in HepG2 cells viability. Combined with previous report[34], the 0.25 mmol/L concentration of PA were applied in the following activity studies (Supporting Information Fig. S1A). Then, we found that JT003 + V14 markedly reduced cellular lipid droplet accumulation, as shown by Oil Red O staining (Fig. 1F and G) and measurement of cellular TG contents (Fig. 1H). In addition, fatty acid metabolism genes, including acyl-CoA dehydrogenase (*Lcad*), peroxisome proliferator-activated receptor alpha (*Ppara*), and peroxisomal acyl-coenzyme A oxidase (*Acox*) (Fig. 1I) were increased and inflammatory gene, including interleukin 6 (*Il-6*), interleukin 1 beta (*Il-1b*), and tumor necrosis factor alpha-like (*Tnfa*) (Fig. 1J) were decreased by JT003 + V14 treatment. Those results are similar with the finding that the levels of gene expression related to lipogenesis (3-hydroxy-3-methylglutaryl-CoA reductase (*HMGCR*), and stearoyl-CoA desaturase 1 (*SCD-1*)) and lipid metabolism (*LCAD*, *PPARa*, and *ACOX*) in PA-induced HepG2 cell, as quantified by qPCR (Fig. S1B). We found that JT003 + V14 is more effective than either JT003 or V14 alone for the prevention of hepatic steatosis and inflammation.

To further examine potential effects of JT003 + V14 on inflammation and lipid metabolism, we performed the RNA-seq analysis in primary hepatocytes. Gene Set Enrichment Analysis (GSEA) biological processes enrichment results show that biological processes associated to lipid metabolism and inflammation were enriched. JT003 + V14 treatment markedly upregulated lipid metabolism and downregulated inflammation process. (Fig. 1K). A heatmap based on the GSEA results further reveals that genes associated to lipid metabolism, and inflammation pathways were significantly upregulated or downregulated, respectively, by JT003 + V14 treatment (Fig. 1L). Altogether, these data indicate that JT003 + V14 might be a useful therapeutic approach to specifically attenuate hepatic steatosis and inflammatory infiltration.
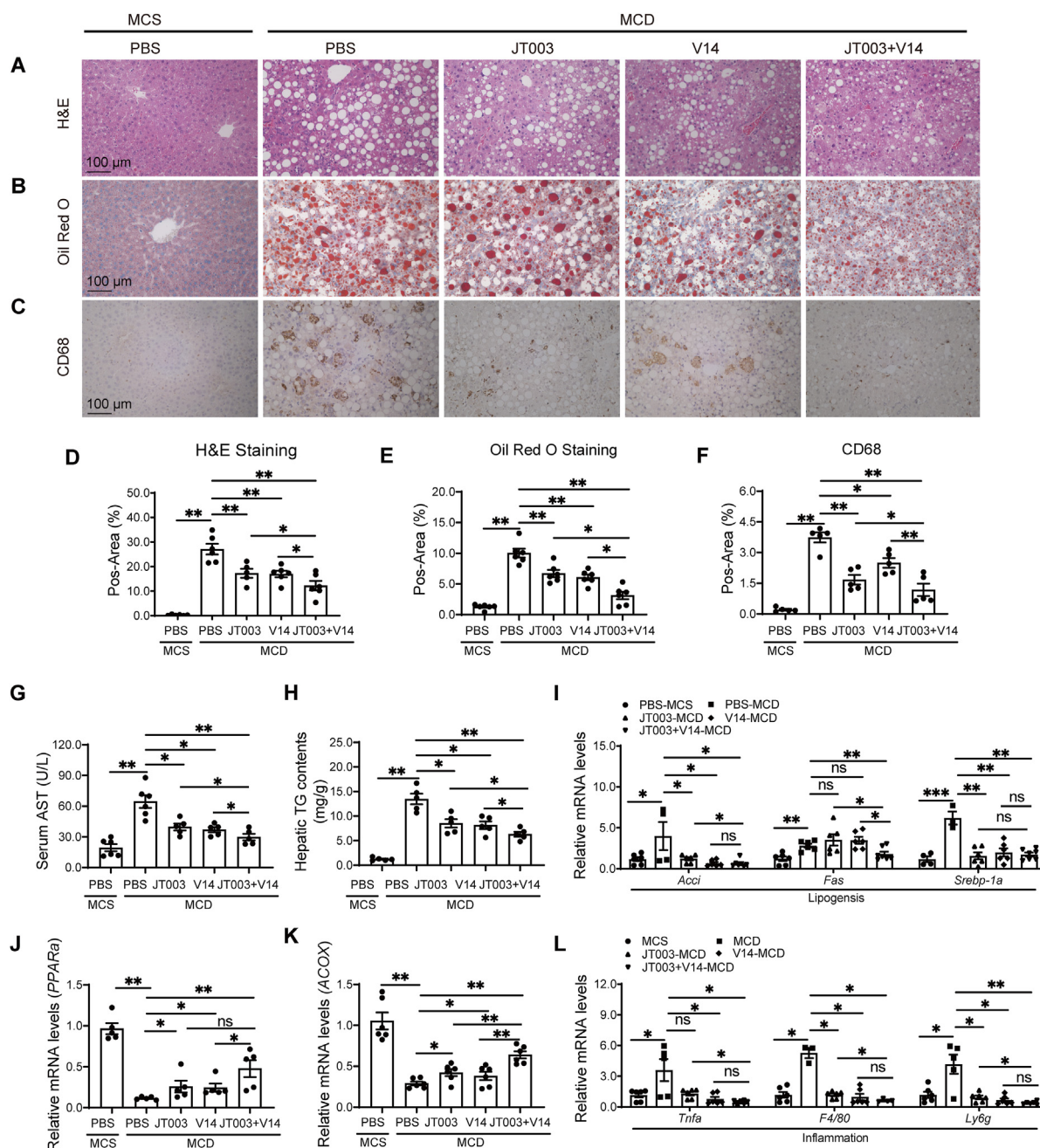
3.2. JT003 + V14 attenuates MCD-induced NASH features

Given the protective effects of JT003 + V14 in *in vitro* assays, we next investigated whether JT003 + V14 also have synergetic effect on the attenuation of hepatic steatosis in mice fed by MCD diet.

First, to detect the potential trends of adiponectin and EDPs levels in NASH model, we analyzed MCD model mice and control mice, using ELISA or Fastin assay, respectively. Compared with control mice, the levels of adiponectin were significantly decreased in model mice (Supporting Information Fig. S2A), while the expression of serum EDPs were slight increase in MCD-fed mice (Fig. S2B). Then, we performed the H&E staining and Oil Red O staining, as expected, the mice fed an MCD diet for 8 weeks exhibited a significantly increase in hepatic steatosis compared to MCS-fed control mice (Fig. 2A). After 4 weeks of treatment, JT003 + V14 markedly reduced hepatic steatosis and inflammatory infiltration showing changes in hepatic sections with H&E staining (Fig. 2A and D), Oil Red O staining (Fig. 2B and E), and immunohistochemistry of CD68 (Fig. 2C and F), as compared to MCD group, JT003 group, and V14 group in MCD-induced NASH mice model. Next, we evaluated serum markers of hepatocellular damage. Compared with mice exposed to JT003 or V14 alone, the cotreatment of JT003 + V14 markedly decreased the AST level (Fig. 2G), and slight decreased the ALT level although this did not reach statistical significance (Fig. S2C). In addition, to further evaluated potential benefits on lipid accumulation and inflammatory infiltration, we assessed changes in hepatic TG contents. JT003 + V14 group displayed lower hepatic TG levels (Fig. 2H). qPCR analyses of the levels of gene expression related to lipogenesis (*Acci*, *Fas*, and *Srebp-1a*) (Fig. 2I), lipid metabolism (*Ppara*, and *Acox*) (Fig. 2J and K), and inflammation (*Tnfa*, *F4/80*, and lymphocyte antigen six complex locus G6D (*Ly6g*)) (Fig. 2L) in the liver tissue, also show the same results as immunohistochemistry staining. Because lipotoxicity eventually contributes to hepatic stellate cell activation and collagen deposition[33], we next examined the expression of collagen using Sirius Red staining. MCD-fed model mice exhibited an increase in collagen deposition compared to control mice. In contrast, these effects were partially reversed by JT003 + V14 (Fig. S2D and S2E). Taken together, these results show that JT003 + V14 attenuates lipid deposition, inflammatory infiltration, hepatocellular damage, and collagen deposition in MCD-induced NASH mice model.

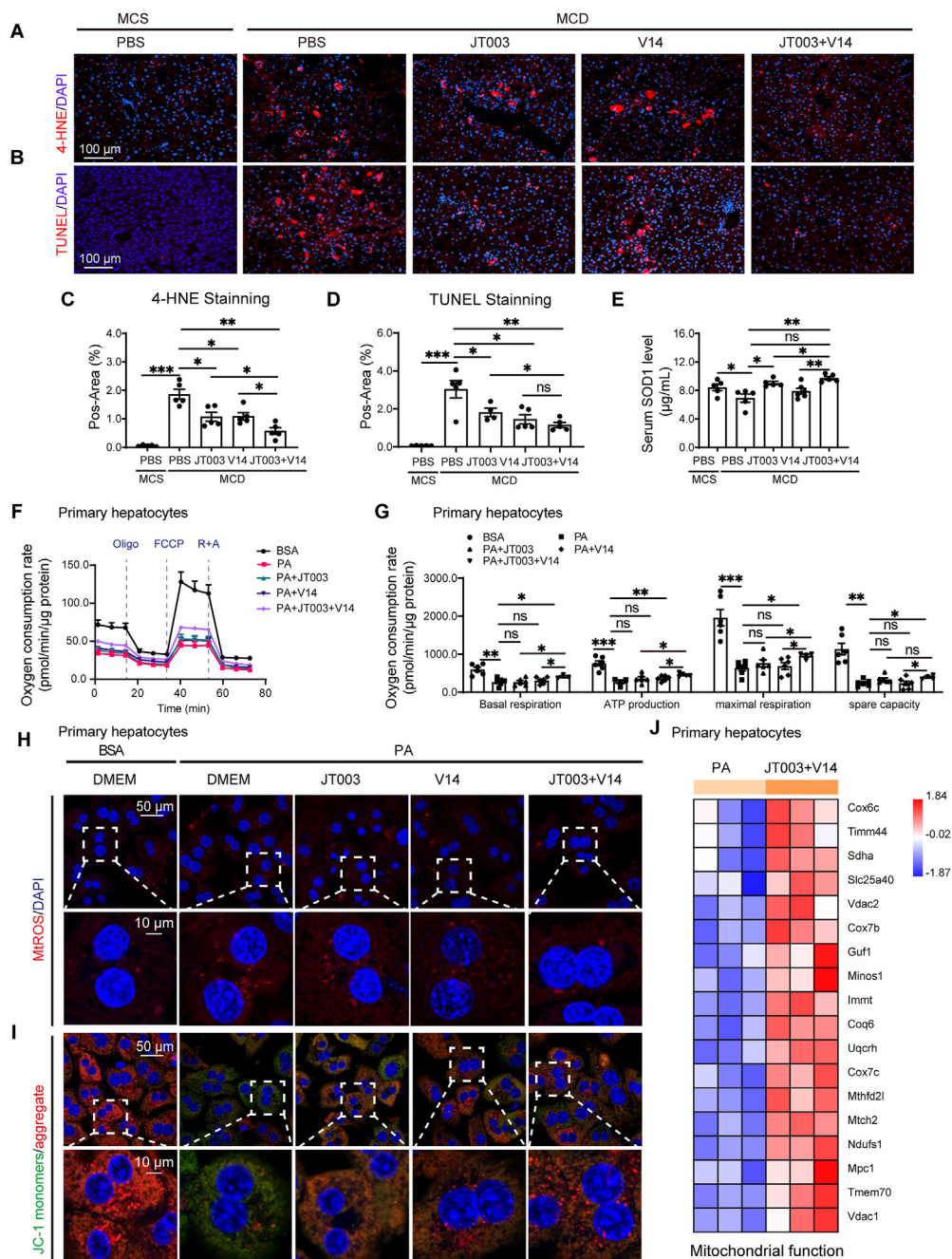### 3.3. JT003 + V14 enhances mitochondrial function in vivo and in vitro

Given that hepatic oxidative stress and mitochondrial dysfunction have been considered as the initial trigger of NAFLD[35−37], we next examined the expression of 4-HNE (a biomarker of hepatic oxidative stress) by immunohistochemistry staining and the number of hepatic apoptosis by TUNEL staining in the liver samples of MCD-fed mice. The result manifested that JT003 + V14 markedly reduced the number of 4-HNE-positive (Fig. 3A and C) and TUNEL-positive cells (Fig. 3B and D) compared to the MCD group, JT003 group, and V14 group. Then, we assessed the marker of antioxidant enzymes by performing kit assay to detect the levels of SOD1 in the serum. The results show that MCD decreased the levels of SOD1 in MCD-induced mice. In contrast, these effects were partially reversed by JT003 + V14 (Fig. 3E). Furthermore, we also evaluated the expression of various oxidative stress genes. Treatment with JT003 + V14 increased the expression of antioxidant enzymes gene in liver tissue, including catalase (*Cat*), *Sod1*, heme oxygenase-1 (*Ho-1*), and glutathione peroxidase 1 (*Gpx1*) (Supporting Informaiton Fig. S3A). Indeed, it is well established that mitochondrial are protected from reactive oxygen species (ROS) by antioxidants[38]. These data demonstrate that JT003 + V14 improves mitochondrial oxidative capacity in MCD-fed mice.

Figure 2 JT003 + V14 attenuates methionine-choline deficient (MCD)-induced non-alcoholic steatohepatitis (NASH) features. (A−C) Representative images of hematoxylin−eosin (H&E) staining ($n = 6$), Oil Red O staining ($n = 6$) and CD68 ($n = 5$) in FFPE sections of livers from mice. (D−F) Image analysis of the positive area of the liver. (G, H) Hepatic TG contents and serum Aspartate transaminase (AST) levels and of mice were measured ($n = 5$). (I−L) mRNA levels of lipogenesis, lipid metabolism and inflammation in the livers from the indicated groups after MCD treatment ($n = 6$). For graphs, all data are represented as mean ± SEM using Dunnett's test as the *post hoc* test following the one-way ANOVA or Tukey's test as the *post hoc* test following the two-way ANOVA. *$P < 0.05$, **$P < 0.01$, ***$P < 0.001$, ns represents no significance.

To further evaluate the effects of JT003 + V14 treatment on mitochondrial function, we performed the OCR assay in primary hepatocytes. Compared to BSA group, PA-treated cells displayed a lower basal respiration, ATP production, maximal respiration, and spare capacity (Fig. 3F and G). In contrast, these effects were partially reversed by JT003 or V14, but that did reach statistical significance only in JT003 + V14 treatment (Fig. 3G). A similar result was observed in the PA-induced HepG2 cells with JT003 + V14 treatment (Fig. S3B and S3C). To investigate the changes in mitochondrial function more closely, the levels of

MitoSOX production and MMP were also assessed. And the results showed that JT003 + V14 treatment markedly attenuated the release of MitoSOX (Fig. 3H) and restored the disrupted MMP (Fig. 3I) in primary hepatocytes. Similar beneficial effects were confirmed in PA-induced HepG2 cells by MitoSOX red staining (Fig. S3D and S3E). The PCR array further show that genes associated with mitochondrial function were upregulated in primary hepatocytes treated with JT003 + V14 (Fig. 3J). Taken together, these results demonstrate that JT003 + V14 reduce oxidative stress and enhance mitochondrial function *in vitro* and *in vivo*.

Figure 3 JT003 + V14 enhance mitochondrial function *in vitro* and *in vivo*. (A, B) Representative images of 4-hydroxynonenal (4-HNE) staining and TdT-mediated dUTP nick end labeling (TUNEL) in FFPE sections of livers from MCD-induced NASH mice. (C, D) Image analysis of the positive area of the liver ($n = 5$). (E) Superoxide dismutase 1 (SOD1) assay to assess hepatic antioxidation in the liver from MCD-induced NASH mice ($n = 5$). (F) Oxygen consumption rate (OCR) assay was performed in primary hepatocytes. (G) Basal respiration, maximal respiration, ATP production, and spare capacity normalized to bovine albumin (BSA)-treated primary hepatocytes ($n = 6$). (H, I) mtROS staining and JC-1 staining in primary hepatocytes treated with PA or JT003 + V14 ($n = 5$). (J) Genes associated to mitochondrial function in microarray analysis from primary hepatocytes ($n = 3$). For graphs, all data are represented as mean ± SEM using Dunnett's test as the *post hoc* test following the one-way ANOVA or Tukey's test as the *post hoc* test following the two-way ANOVA. $*P < 0.05$, $**P < 0.01$, $***P < 0.001$, ns represents no significance.

3.4 JT003 + V14 induces mitochondrial mitophagy and biogenesis in primary hepatocytes and MCD-induced NASH model

It is reported that ROS induced autophagy, and which, in turn, serves to reduce oxidative damage[39]. Next, we examined whether JT003 + V14 induce autophagy. Transmission electron microscope analyses showed that autophagosome were frequently observed by JT003 + V14 treatment in PA-induced primary hepatocytes (Fig. 4A). Next, we assessed the levels of LC3II/I and the degradation of the autophagy receptor P62 by Western blotting in PA-induced primary hepatocytes. We found that autophagic flux was obviously induced by the increased the ratio of
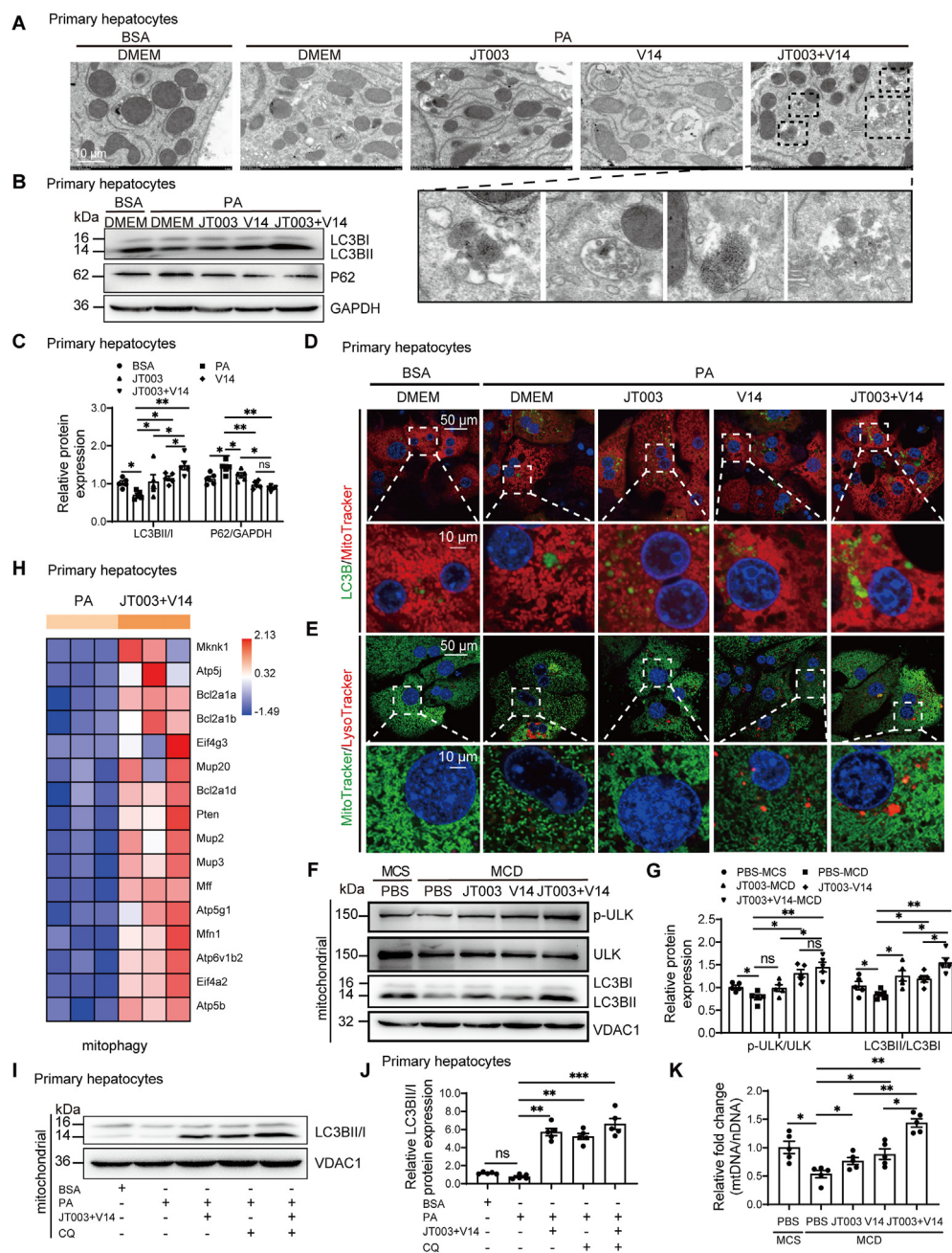
Figure 4 JT003 + V14 induces mitochondrial mitophagy and biogenesis *in vitro* and *in vivo*. (A) Images of electron microscopy analyses in primary hepatocytes treated with PA or JT003 + V14 ($n = 5$). (B, C) The ratio of microtubule-associated protein 1 light chain 3 (LC3BII/I) and sequestosome 1 (P62) protein expression levels were measured using Western blot (WB) in the PA-induced primary hepatocytes ($n = 5$). (D) Confocal microscopy in primary hepatocytes treated with PA or JT003 + V14, LC3 protein was detected by GFP, and mitochondria were detected by MitoTracker® Red FM ($n = 5$). (E) Confocal microscopy in primary hepatocytes, lysosome was detected by Lyso-Tracker Red FM and mitochondria were detected by MitoTracker® Green FM ($n = 5$). (F, G) Unc-51-like kinase 1 (ULK) phosphorylation and the ratio of LC3BII/I levels in the mitochondrion were measured using WB in the MCD-induced NASH models ($n = 5$). (H) Genes associated to mitophagy in microarray analysis from primary hepatocytes treated with PA or JT003 + V14 ($n = 3$). (I, J) The ratio of LC3BII/I were measured using WB in the PA-induced primary hepatocytes with chloroquine (CQ) ($n = 5$). (K) mtDNA copy number as evaluated by qPCR decreased by JT003 + V14 treatment in MCD-induced NASH model ($n = 5$). For graphs, all data are represented as mean ± SEM using Dunnett's test as the *post hoc* test following the one-way ANOVA or Tukey's test as the *post hoc* test following the two-way ANOVA. *$P < 0.05$, **$P < 0.01$, ***$P < 0.001$, ns represents no significance.

LC3BII/I and decreased the levels of P62 in JT003 + V14 group, as compared to PA group, JT003 group, or V14 group (Fig. 4B and C). CQ, a pharmacological inhibitor of blocking the fusion of the autophagosome with lysosome, caused LC3BII accumulation[40]. To further study whether JT003 + V14 induced autophagy,

we measured the turnover of GFP-LC3B after CQ treatment by using a flow cytometry-based assay for autophagy[41]. The results showed that a markedly increase in the level of GFP-LC3 was observed after 6 h of JT003 + V14 or CQ treatment in fluorescence and treatment of JT003 + V14 with CQ further increase in

the fluorescence signal, indicating that JT003 + V14 activate autophagy in primary hepatocytes (Supporting Information Fig. S4A). In addition, the levels of autophagy-related proteins autophagy-related 5 (ATG5) and BCL2 interacting protein 3 (BNIP3) (Fig. S4B and S4C) and genes involved in autophagy, including mechanistic target of rapamycin kinase (*mTor*), *P62*, microtubule-associated protein 1 light chain 3 (*Lc3b*), autophagy-related 7 (*Atg7*), parkin RBRE3 ubiquitin-protein ligase (*Park2*), and BCL2 interacting protein 3 like (*Bnip3l*) (Fig. S4D), were also induced by JT003 + V14 treatment in MCD-induced NASH model. Taken together, these results indicate that JT003 + V14 induced autophagy in primary hepatocytes and in MCD-induced NASH model.

Next, we determined whether JT003 + V14 can induce mitophagy. The electron microscopy analyses revealed that JT003 + V14 increased the colocalization of GFP-tagged LC3B with MitoTracker red both in primary hepatocytes (Fig. 4D) and HepG2 cells (Fig. S4E). To further confirm these observations, we evaluated the level of colocalization between LysoTracker and MitoTracker green in primary hepatocytes (Fig. 4E) and HepG2 cells (Fig. S4F) and found that JT003 + V14-treated cells exhibited an obviously higher number of lysosomes that co-localized with mitochondria. Moreover, we detected changes in autophagy related protein in mitochondria after JT003 + V14 treatment in MCD-induced NASH mice by Western blotting for the Unc-51-like kinase 1 (ULK) and LC3BII and found that a marked increase of ULK phosphorylation and LC3BII accumulation by JT003 + V14 treatment, indicating an induction of mitophagy (Fig. 4F and G). To further investigate mitophagy, mitochondrial LC3BII accumulation was detected in the primary hepatocytes treated with or without CQ after JT003 + V14 treatment. And we found that when CQ was added together with JT003 + V14, there was a further increase in mitochondrial LC3BII level compared to group treated with JT003 + V14 alone (Fig. 4I and J), strongly suggesting that mitophagy flux was induced by JT003 + V14. Moreover, the PCR array showed that genes associated with mitophagy were upregulated in primary hepatocytes treated with JT003 + V14 (Fig. 4H). Overall, these results indicate that JT003 + V14 induced complete mitophagy in primary hepatocytes and MCD-induced NASH model.

We determined whether JT003 + V14 can induced mitochondrial biogenesis and analyzed mitochondrial DNA (mtDNA) copy number by measuring the ratio of mitochondrial over nuclear DNA (mt/nNDA). We found that JT003 + V14 increased mtDNA copies in MCD-induced NASH model (Fig. 4K). Similar results were observed in PA-induced HepG2 cells model (Fig. S4G). Then, we assessed markers of mitochondrial biogenesis by qPCR assay to detect the gene expression of nuclear respiratory factor 1 (*Nrf1*) and immunoreceptor tyrosine-based activation motif (*Itam*) in the liver tissues. The results showed that MCD decreased the *Nrf1* and *Itam* gene levels (Fig. S4H). Moreover, we also found that the level of PGC1α protein expression were obviously elevated in JT003 + V14-induced group in comparison with the other groups in mice (Fig. S4I and S4J). These results indicate that JT003 + V14 induced mitochondrial biogenesis in HepG2 cells and MCD-induced NASH model.

3.5. JT003 + V14 attenuates HFD-induced NASH features

To further investigate the protective effects of JT003 + V14 combined therapy against NASH *in vivo*, we next established an HFD-induced NASH mouse model that mimic the pathologic features of patients with NASH. Compared with control mice, the levels of adiponectin were significantly decreased in HFD-induced mice, while the expression of serum EDPs were increased in mice (Supporting Information Fig. S5A and S5B). H&E (Fig. 5A and D), Oil Red O (Fig. 5B and E) staining and immunohistochemistry of CD68 (Fig. 5C and F) show that both steatosis and inflammatory response signatures were notably attenuated in mice treated with JT003 + V14 combination compared with that of JT003, V14, or vehicle treatment alone. Moreover, JT003 + V14 decreased the serum levels of AST and ALT in HFD-induced NASH models (Fig. 5G, and Fig. S5C), indicating that JT003 + V14 improve the hepatocellular damage. In addition, we observed increased the expression of genes involved in lipid metabolism (*Ppara*, and pyruvate dehydrogenase kinase 4 (*Pdk4*)) (Fig. 5H) and reduced the expression of genes involved in inflammation (*Tnfa* and *F4/80*) (Fig. 5I) by JT003 + V14 treatment in HFD-induced mice. We next examined the expression of collagen using Sirius Red staining. HFD-fed model mice exhibited an increase in collagen deposition compared to control mice. In contrast, these effects were partially reversed by JT003 + V14 (Fig. S5D and S5E). Taken together, these results indicate that JT003 + V14 treatment prevents hepatic inflammation and hepatic lipid accumulation in HFD-fed mice.

3.6. JT003 + V14 induces mitophagy and enhances mitochondrial function in HFD-fed mice

Having shown the results in MCD-fed NASH mouse model, we performed the ROS and TUNEL staining to detect the levels of ROS and hepatic apoptosis in HFD-induced NASH mice. The results reveal that JT003 + V14 could reduce ROS contents (Fig. 6A and C) and hepatic apoptosis (Fig. 6B and D). We next assessed various antioxidant enzymes genes by qPCR assay and found that treatment JT003 + V14 elevated the expression of *Cat*, *Sod1*, *Ho-1*, and *Gpx1* in mice (Supporting Information Fig. S6A). What's more, administration of JT003 + V14 was also related with a decrease in mRNA expression of a subset of oxidation-reduction and apoptosis genes (Fig. 6E). Overall, these results indicate that JT003 + V14 improves mitochondrial oxidative capacity and reduced the hepatic apoptosis in MCD-fed NASH mouse model.

Electron microscopy analyses revealed that autophagosome and isolation membranes were frequently observed were increased in HFD mice treated with JT003 + V14, indicating that the autophagosome formation were induced by JT003 + V14 (Fig. 6F). qPCR analyses of the expression of autophagy in the liver, including *Bnip3*, and *mTor* (Fig. 6G and H), also show the same results as electron microscopy. To determine whether JT003 + V14 could induced mitophagy in HFD-induced NASH model, we assessed changes in p-ULK and LC3BII/I in mitochondria of liver tissue. The results show that JT003 + V14 increased the levels of p-ULK and the ratio of LC3BII/I in mice treated with JT003 + V14 (Fig. 6I and J). In agreement with the increased mitophagy-related protein, a heatmap results further revealed a significant enhance in mitophagy, indicating that mitophagy was enhanced in HFD mice treated with JT003 + V14 (Fig. 6K).

To measure whether JT003 + V14 could enhance mitochondrial biogenesis in HFD-induced NASH model, we measured the protein expression levels of PGC1α in the liver tissue by Western blotting. The result shows that JT003 + V14 could significantly
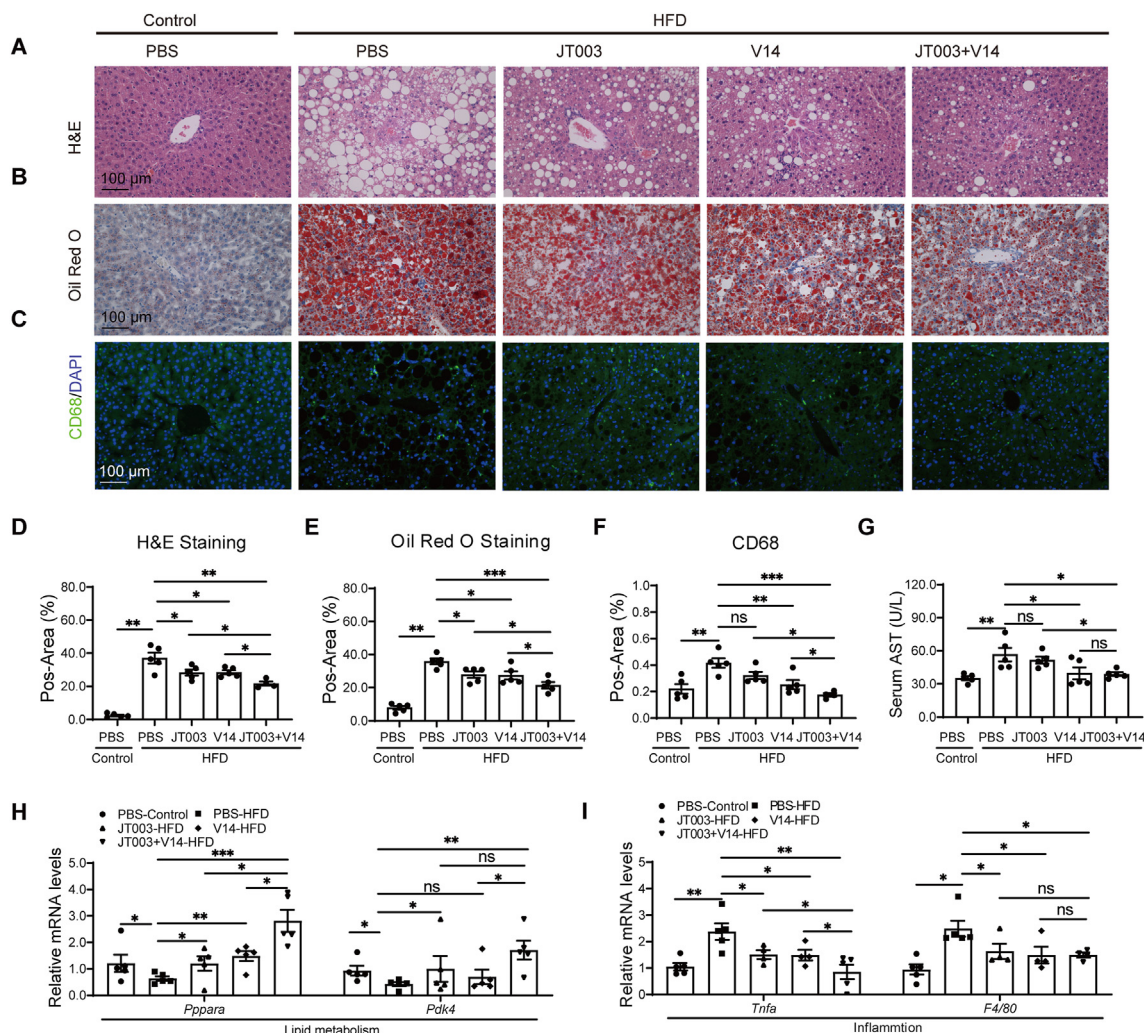
Figure 5 JT003 + V14 attenuates high fat diet (HFD)-induced NASH features. (A−C) Representative images of H&E staining, Oil Red O staining, and IHC of CD68 in FFPE sections of livers in HFD-induced NASH. (D−F) Image analysis of the positive area of the liver from HFD-induced NASH mice ($n = 5$). (G) Serum levels of AST of mice were measured in NASH mice that fed an HFD ($n = 5$). (H, I) mRNA levels of lipid metabolism and inflammation in the livers from the indicated groups after HFD treatment ($n = 5$). For graphs, all data are represented as mean ± SEM using Dunnett's test as the *post hoc* test following the one-way ANOVA or Tukey's test as the *post hoc* test following the two-way ANOVA. *$P < 0.05$, **$P < 0.01$, ***$P < 0.001$, ns represents no significance.

increase the expression of PGC1α compared with JT003 or V14 alone (Fig. 6L and M). The results of mtDNA copy number analysis show that JT003 + V14 treatment significantly increased liver mtDNA copy number in HFD-induced NASH model (Fig. 6N).

Taken together, these results indicate that JT003 + V14 ameliorates oxidative stress, induces mitophagy and increases mitochondrial biogenesis in HFD-induced NASH model.

3.7. JT003 + V14 attenuates CCl₄-induced liver fibrosis in mice

Fibrosis is characterized by excessive deposition of extracellular matrix, which can induce organ dysfunction[42,43]. Encouraged by the in HFD or MCD-induced NASH model results, we used a CCl₄-induced liver fibrosis model to assess the effect of JT003 + V14 on liver fibrosis and inflammation. Compared with Oil mice, the levels of adiponectin were significantly decreased in CCl₄-induced mice, while the expression of serum EDPs were increased in mice (Supporting Information Fig. S7A and S7B). H&E (Fig. 7A), Sirius Red (Fig. 7B and F) and

immunohistochemistry of CD68 (Fig. 7C and G) staining show that JT003 + V14 remarkably reduced collagen deposition and inflammatory cell infiltration in mice induced by CCl₄. Then, we evaluated makers of liver fibrogenesis by detecting the levels of Col1α in the liver tissue. The results reveal that the Col1α (Supporting Information Fig. S8A and S8B) levels are significantly lower in the JT003 + V14 group than in CCl₄ group, JT003 group, or V14 group, indicating that JT003 + V14 prevented the progression of liver fibrosis. Additionally, JT003 + V14 decreased the levels of ECM metabolism genes (*Col1a*, and *Timp1*) (Fig. 7J) and inflammatory cytokines genes (*Il-6*, *iNos*, and *Ly6g*) (Fig. 7K), which were upregulated in CCl₄-treated mice. We evaluated serum markers of hepatocellular damage. The results show that the ALT and AST levels were significantly elevated in the CCl₄-treated group in comparison with the control group. And JT003 + V14 treatment decreased the levels of these biomarkers (Fig. 7L and M). Overall, JT003 + V14 improves liver injury, collagen accumulation and hepatic stellate cell activation.

Similar to the results obtained with the MCD fed NASH model, JT003 + V14 significantly decreased the hepatic 4-HNE
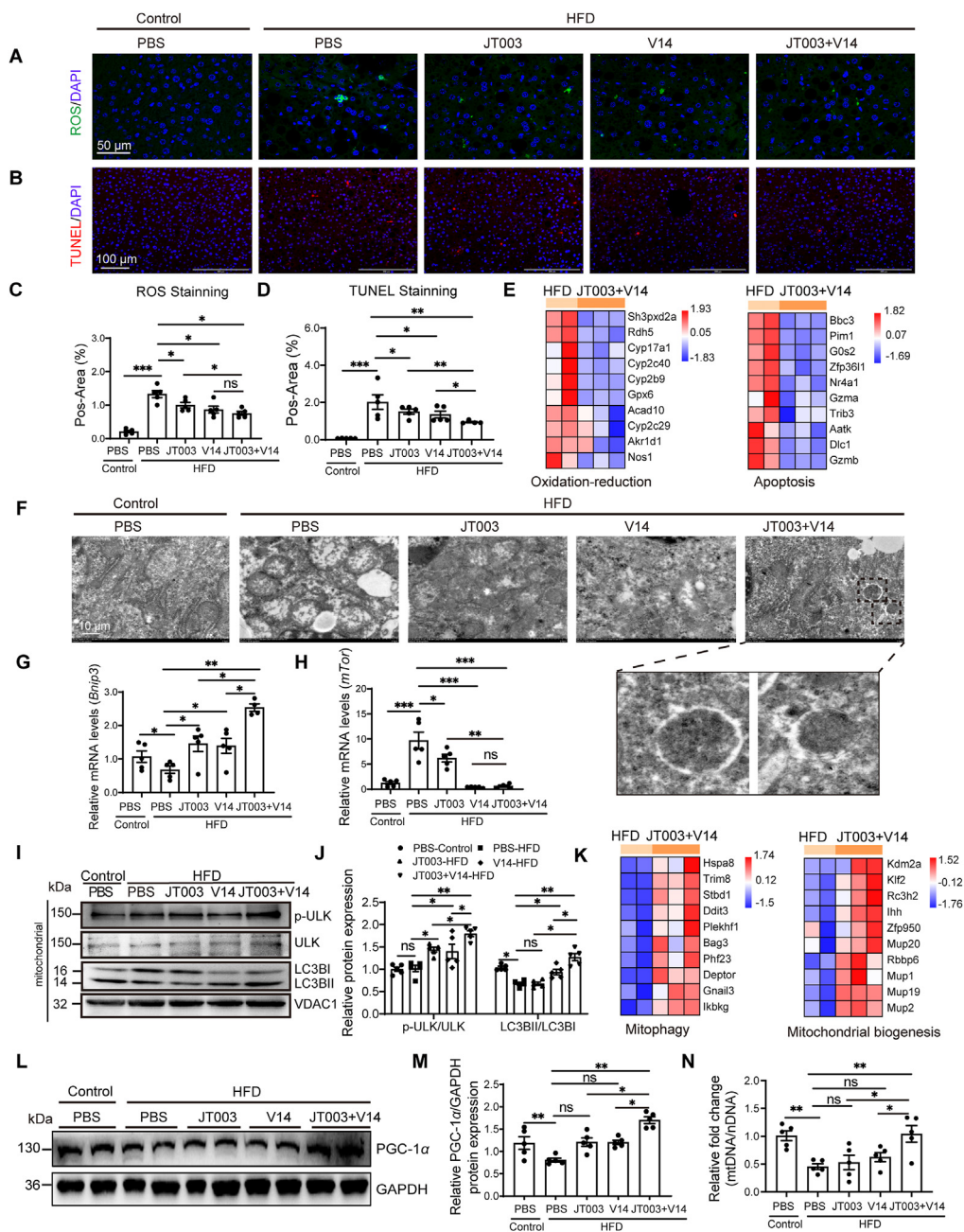
Figure 6 JT003 + V14 enhance mitochondrial function and turnover in HFD mice. (A, B) ROS staining and TUNEL staining of liver sections in HFD-induced NASH mice. (C, D) Image analysis of the positive area of the liver from HFD-induced NASH mice ($n = 5$). (E) Genes associated to oxidation, reduction, and apoptosis in microarray analysis from the liver of NASH mice that fed an HFD ($n = 3$). (F) Representative images of electron microscopy analyses in HFD mice ($n = 3$). (G, H) mRNA levels of mitophagy (*Bnip3*, *mTor*) in the livers from the HFD-induced NASH mice ($n = 5$). (I, J) ULK phosphorylation and the ratio of LC3BII/I levels in the mitochondrion were measured using WB in HFD mice ($n = 5$). (K) Genes associated to mitophagy and mitochondrial biogenesis in microarray analysis from the liver of NASH mice that fed an HFD ($n = 3$). (L, M) WB analysis of peroxisome proliferator-activated receptor-gamma coactivator (PGC)-1α in MCD-induced NASH models ($n = 5$). (N) mtDNA copy number as evaluated by qPCR decreased by JT003 + V14 treatment ($n = 5$). For graphs, all data are represented as mean ± SEM using Dunnett's test as the *post hoc* test following the one-way ANOVA or Tukey's test as the *post hoc* test following the two-way ANOVA. *$P < 0.05$, **$P < 0.01$, ***$P < 0.001$, ns represents no significance.

contents (Fig. 7D and H) and hepatic apoptosis (Fig. 7E and I) in CCl₄-induced liver fibrosis. The levels of serum glutathione (GSH) (Fig. 7N) and SOD (Fig. 7O) were enhanced in CCl₄ mice treatment with JT003 + V14, indicating that JT003 + V14 improve oxidative stress. Together, these data indicate that JT003 + V14 attenuates liver fibrosis, inflammation, and oxidative stress, exerting potent anti-fibrosis effects.

3.8. JT003 + V14 improves mitochondrial function by activating the AMPK pathway

It has been demonstrated that AMPK is the co-downstream protein of EDPs and adiponectin[27,44]. We next investigated whether JT003 + V14 treatment enhances mitochondrial function and mitochondria respiration dependent on AMPK activation. We
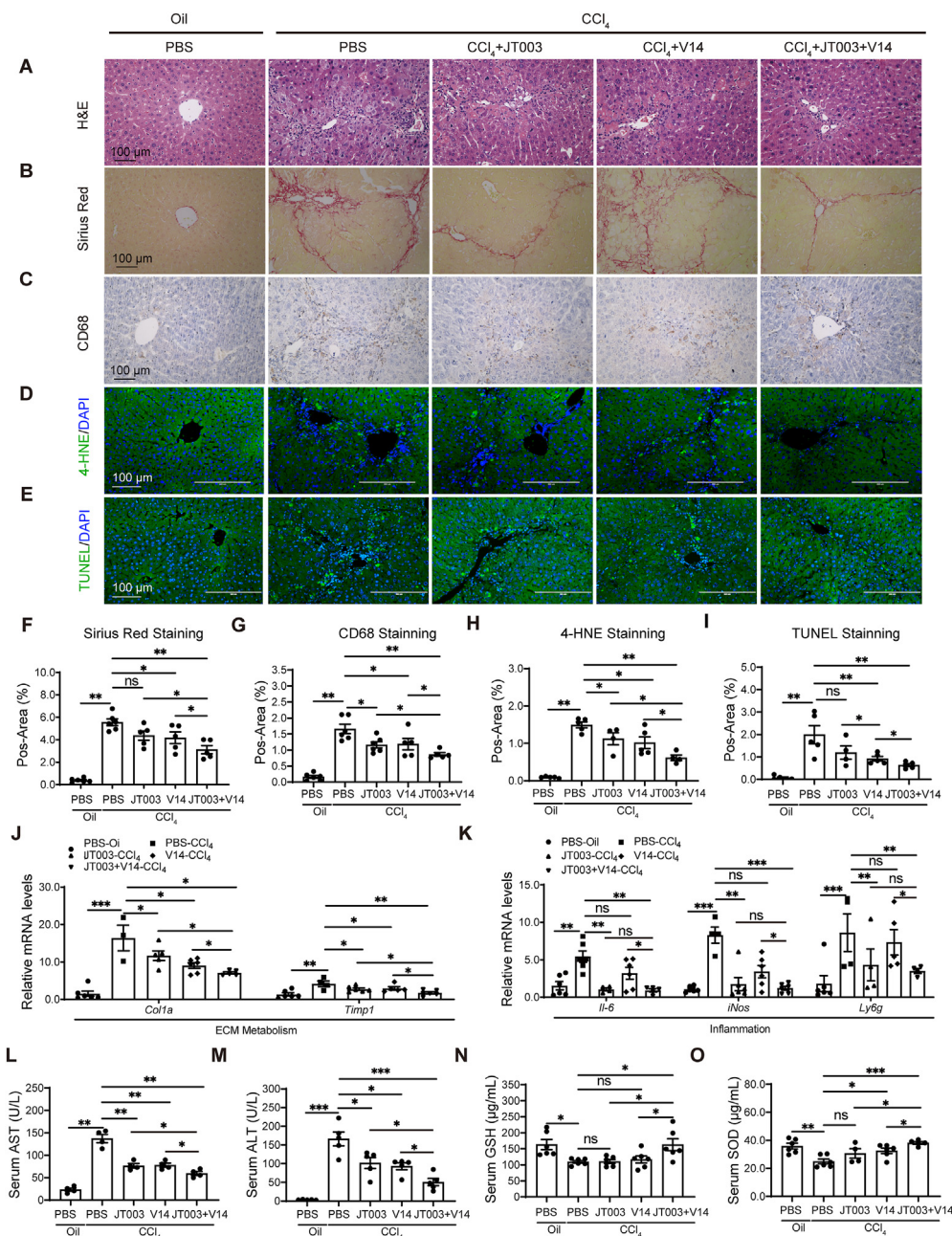
Figure 7 JT003 + V14 inhibit the progress of carbon tetrachloride (CCl$_4$)-induced liver fibrosis. (A−C) H&E, Sirius Red staining and IHC of CD68 in FFPE sections of the livers form the CCl$_4$-induced mice. (D, E) ROS staining and TUNEL staining of liver sections. (F−I) Image analysis of the positive area of Sirius Red staining, CD68 staining, 4-HNE staining and TUNEL staining ($n = 5$). (J, K) qPCR of gene linked to extracellular matrix (ECM) metabolism and inflammation in liver tissue ($n = 5$). (L−O) AST, ALT, glutathione (GSH) and SOD levels in serum were analyzed in CCl$_4$-induced NASH mice ($n = 5$). For graphs, all data are represented as mean ± SEM using Dunnett's test as the *post hoc* test following the one-way ANOVA or Tukey's test as the *post hoc* test following the two-way ANOVA. *$P < 0.05$, **$P < 0.01$, ***$P < 0.001$, ns represents no significance.

found that AMPK phosphorylation was notably upregulation *in vitro* and *in vivo* (Fig. 8A; Supporting Information Fig S9A−S9C). In addition, to examine whether AMPK phosphorylation is necessary for JT003 + V14 to improve mitochondrial function, we used the AMPK inhibitor, compound C, to block AMPK activation in primary hepatocytes. We found that specifically suppressed AMPK by compound C blocked increased maximal respiratory rates by JT003 + V14 treatment (Fig. 8C−F) and decreased mtROS contents (Fig. 8G) in primary hepatocytes,

indicating that JT003 + V14 improve oxidative stress and enhances mitochondrial function *via* AMPK pathways.

To further confirm the enhancement effects of JT003 + V14 on autophagy *via* AMPK pathways, we evaluated the levels of autophagosome formation by electron microscopy analysis. We found that autophagosome and isolation membranes were almost abrogated in primary hepatocytes by pretreatment with compound C (Fig. 8B), indicating that JT003 + V14 induced autophagy *via* AMPK pathways.
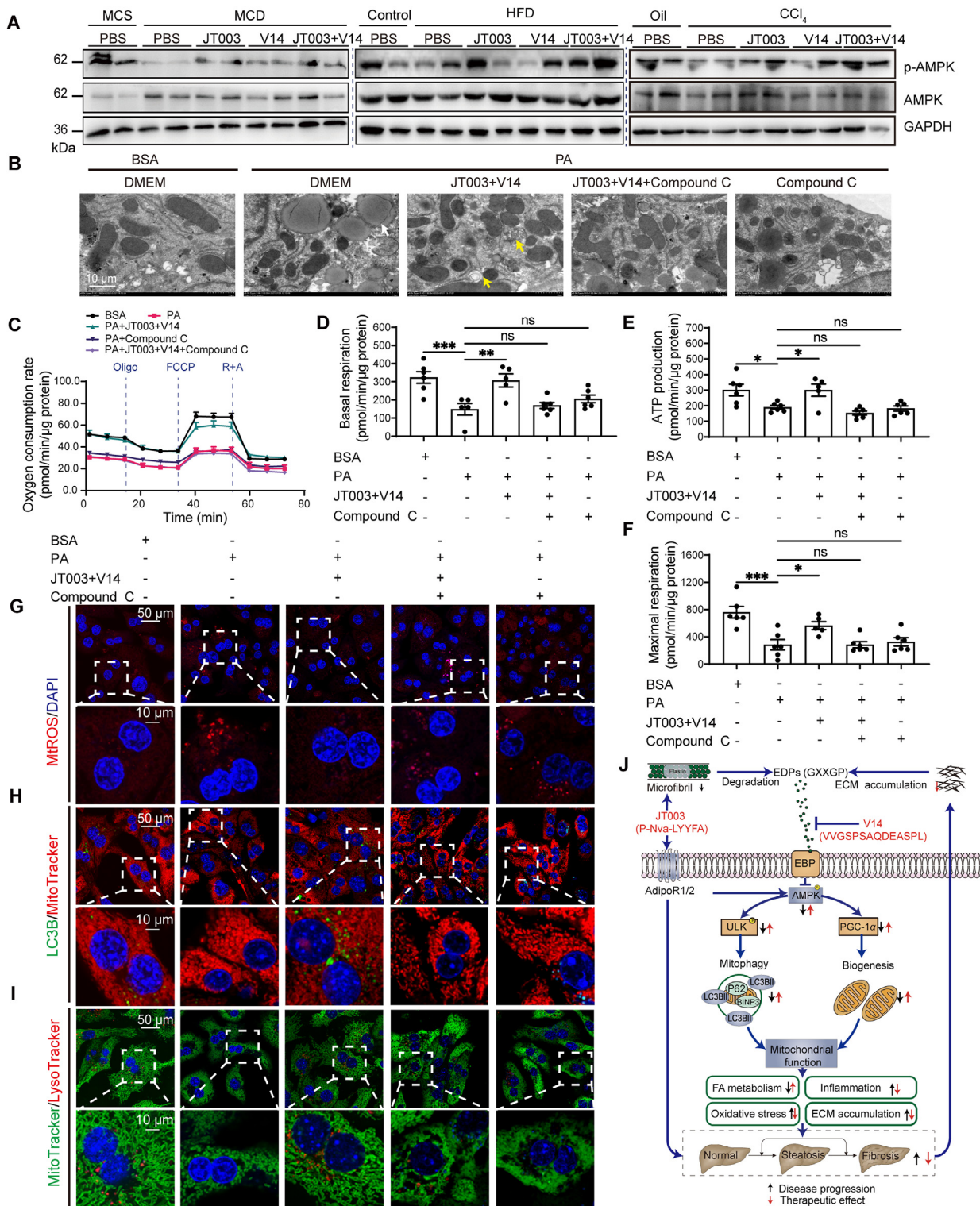
Figure 8 Decreased mitophagy and mitochondrial biogenesis by compound C in PA-induced primary hepatocytes. (A) Representative WB analysis for adenosine monophosphate-activated protein kinase (AMPK) expression in the livers of MCD, HFD, and CCl₄-induced mice ($n = 5$). (B) Representative images of electron microscopy analyses in primary hepatocytes with compound C ($n = 5$), lipid drops were marked by the white arrow and autophagosome as well as isolation membranes were marked by yellow arrow. (C) OCR was analyzed in primary hepatocytes treated with compound C ($n = 5$). (D–F) Basal respiration, maximal respiration, and ATP production normalized to BSA-treated primary hepatocytes ($n = 5$). (G) Representative images of mtROS staining treated with compound C in primary hepatocytes treated with compound C ($n = 5$). (H) Confocal microscopy of mitophagy in primary hepatocytes treated with compound C. LC3 protein was detected by GFP, and mitochondria were detected by MitoTracker® Red FM ($n = 5$). (I) Confocal microscopy in primary hepatocytes, lysosome was detected by Lyso-Tracker Red FM and mitochondria were detected by MitoTracker® Green FM ($n = 5$). (J) Scheme of JT003 + V14 in recovering NAFLD. For graphs, all data are represented as mean ± SEM using Dunnett's test as the *post hoc* test following the one-way ANOVA or Tukey's test as the *post hoc* test following the two-way ANOVA. *$P < 0.05$, **$P < 0.01$, ***$P < 0.001$, ns represents no significance.

Immunofluorescent staining shows that co-localization of mitochondria within LC3B or lysosome and number of mitochondria were decreased by compound C, which was unable to be recovered by JT003 + V14 treatment in primary hepatocytes (Fig. 8H and I) and HepG2 cells (Fig. S9D and S9E). Additionally, suppression of AMPK reduced the increase of the ULK phosphorylation, LC3BII/I ration and PGC1α level by JT003 + V14 in HepG2 cells, which was also unable to be recovered by JT003 + V14 treatment (Fig. S9F and S9G), indicating that JT003 + V14 combination promotes hepatocyte mitophagy through activation of AMPK pathways in hepatocytes under metabolic stress condition. We explored whether the upregulation of AMPK phosphorylation was associated with EDPs−ERC pathways by using an EBP inhibitor chondroitin sulfate (CS). The results show that combined of JT003 and CS can markedly enhance the expression of AMPK phosphorylation in HepG2 cells, that is similar to combined of JT003 and V14 (Supporting Information Fig. S10A), suggesting that combination JT003 and V14 upregulate AMPK phosphorylation most likely through influence EBP. Collectively, these data reveal that suppression of AMPK completely eliminates the protective effects of JT003 + V14 therapy on reduces oxidative, mitochondrial function, mitophagy and mitochondrial biogenesis, indicating that the therapeutic effects of JT003 + V14 dependent on activation of AMPK pathway.

4. Discussion

In this study, we demonstrated that a JT003 + V14 exerts a positive synergistic lipid-lowering and fibrosis-lowing effect *in vitro* and *in vivo*. To clarify the effects of JT003 + V14 on NAFLD disease, we have performed a series of *in vitro* and *in vivo* studies. Monounsaturated OA was less toxic in hepatocytes and PA can induced a change in mitochondrial membrane potential, which is considered to be very early event of NASH[45]. Therefore, it was decided to evaluate the effect of combination of JT003 and V14 on NASH *in vitro* treated with PA rather than OA. We observed that JT003 + V14 reduced hepatic steatosis, inflammatory infiltration and fibrosis in multiple models, in addition to enhanced mitochondrial oxidative capacity, improved mitochondrial biogenesis and mitophagy. Furthermore, suppression of AMPK completely eliminates the protective effects of JT003 + V14 on mitochondrial dysfunction, indicating that the therapeutic effects of JT003 + V14 dependent on activating AMPK phosphorylation. Taken together, our findings indicated that a JT003 + V14 is more effective than either alone in attenuating NASH and liver fibrosis in rodent by enhancing mitochondrial function and improving mitochondrial oxidative capacity *via* AMPK pathways *in vitro* and *in vivo* (Fig. 8J).

Several studies in related fields clearly demonstrated that the adiponectin and EDPs were involved in NAFLD progression[27,46]. Likewise, we quantitated levels of adiponectin and elastin in the human liver tissues and plasma, and the results confirmed that there have a lower adiponectin levels and higher elastin expression in patient with fibrosis than healthy volunteers, indicating that JT003 + V14 is beneficial for exertion of maximum therapeutic efficiency. In this presents study, JT003 + V14 improved inflammation and increased lipid β-oxidation along with a reduction of hepatic apoptosis and ROS production. The effects on intracellular triglycerides are likely complex as JT003 + V14 decreased lipogenesis but also impacts lipid β-oxidation and mitochondrial function, directly or indirectly. Interestingly, our data show a markedly enrich of genes in lipid β-oxidation and mitochondrial turnover. Herein, we demonstrate that JT003 + V14 enhanced mitochondrial turnover and homeostasis, as demonstrated by increasing mitochondrial membrane potential and oxygen consumption, resulting in an overall more robust mitochondrial population reflected by increased oxidative capacity. Collectively, this indicates that increased lipid β-oxidation along with decreased inflammation is mediated through the improved mitochondrial turnover and enhanced mitochondrial function.

It is reported that JT003 and V14 are all involved in AMPK phosphorylation[23,27], which has identified as a vital metabolic switch, which regulates multiple processes involved in lipid metabolism, and energy[47]. In this present study, we found that JT003 + V14 treatment improve mitochondrial turnover reflected by increased mitophagy and mitochondrial biogenesis. Moreover, JT003 + V14 significantly increased the expression of PGC1α and ULK, which are the main downstream targets of AMPK, indicating AMPK signals may be activated. It has been previously reported that AMPK responds to energy stress by inducing mitochondrial biogenesis and mitophagy[48,49], in part through its promotion of the PGC1α and ULK pathways[50]. It is noteworthy, we found that JT003, V14, or JT003 + V14 treatment increase AMPK phosphorylation *in vivo* and did reach statistical significance. These data support by studies in JT003 + V14 treatment mice point to the results of JT003 + V14 increased mitophagy and mitochondrial biogenesis *via* AMPK pathways. In addition, we found that more importantly, pharmacological inhibition of AMPK signaling blocked both the elevated mitochondrial homeostasis and turnover induced by JT003 + V14 treatment, indicating the effect of JT003 + V14 on mitochondria was mediated by the AMPK. The activation of AMPK signals by JT003 + V14 largely enhanced lipid β-oxidation and reduced lipogenesis *in vivo* and *in vitro*. This enhancement may be attributed to the activation of acetyl CoA carboxylase pathways which is the downstream of AMPK (Supporting Information Fig. S11A and S11B). However, not the obviously changes of body weight were observed after JT003, V14 or JT003 + V14 treatment in MCD-induced NASH model and CCl₄-induced liver fibrosis model (Supporting Information Fig. S12A and S12B). The possible reason is that the dose and/or timing of these peptides administration in our experiments may not be optimal for losing body weight.

Our studies have three potential advantages: (i) The combination of JT003 and V14 could directly counteract the low expression of adiponectin and accumulation of EDPs in the disease process. (ii) Combination of JT003 and V14 possessed excellent synergistic effects on NASH and liver fibrosis since they compensate the shortage of each other. (iii) The combination of AdipoR1/2 dual agonist and inhibitor of EDPs−EBP interaction has not been applied in NAFLD, and the current study provides an effective alternative treatment strategy against NASH and liver fibrosis in this field. Our studies also have limitations, for example, combination therapy would increase the pain of administration, while it would be a better choice if the two drugs were made into a compound preparation or a coupled drug.

Taken together, the beneficial effects of JT003 + V14 in improving steatosis and fibrosis by increasing β-oxidation and decreasing inflammation are likely related to its ability to modulate mitochondrial function including mitochondrial homeostasis, oxygen consumption, mitophagy, and mitochondrial

biogenesis. In conclusion, the synergetic effects of JT003 and V14 therapy exert a positive synergistic lipid-lowering and fibrosis-lowing effect. It may be a potential strategy to prevent NAFLD progression and provide a new theoretical basis for NAFLD.

Author contributions

Xianxing Jiang and Rui wang conceived and designed the research and supervised the studies. Nazi Song and Hongjiao Xu performed the experiments and analyzed data. Shuohan Wu supported the peptide synthesis and purification. Suijia Luo and Jingyao Xu performed the cell experiments and the acquisition of data. Shuohan Wu and Qian Zhao and performed the AMPK inhibitor assay. Xianxing Jiang and Nazi Song analyzed the data and wrote the manuscript.

Conflicts of interest

The authors declare no conflicts of interest.

Appendix A.   Supporting information

Supporting data to this article can be found online at https://doi.org/10.1016/j.apsb.2022.10.003.

References

1. Wree A, Broderick L, Canbay A, Hoffman HM, Feldstein AE. From NAFLD to NASH to cirrhosis—new insights into disease mechanisms. *Nat Rev Gastroenterol Hepatol* 2013;**10**:627−36.
2. Friedman SL, Neuschwander-Tetri BA, Rinella M, Sanyal AJ. Mechanisms of NAFLD development and therapeutic strategies. *Nat Med* 2018;**24**:908−22.
3. Wu L, Guo C, Wu J. Therapeutic potential of PPARγ natural agonists in liver diseases. *J Cell Mol Med* 2020;**24**:2736−48.
4. Preidis GA, Kim KH, Moore DD. Nutrient-sensing nuclear receptors PPARα and FXR control liver energy balance. *J Clin Invest* 2017;**127**:1193−201.
5. Huang DQ, El-Serag HB, Loomba R. Global epidemiology of NAFLD-related HCC: trends, predictions, risk factors and prevention. *Nat Rev Gastroenterol Hepatol* 2021;**18**:223−38.
6. Ratziu V, Harrison SA, Francque S, Bedossa P, Lehert P, Serfaty L, et al. Elafibranor, an agonist of the peroxisome proliferator-activated receptor-α and -δ, induces resolution of nonalcoholic steatohepatitis without fibrosis worsening. *Gastroenterology* 2016;**150**:1147−1159.e5.
7. Intercept Pharmaceuticals, Inc.. Intercept receives complete response letter from FDA for obeticholic acid for the treatment of fibrosis due to NASH. Globenewswire; June 29, 2020. Available from: https://www.globenewswire.com/news-release/2020/06/29/2054576/0/en/Intercept-Receives-Complete-Response-Letter-from-FDA-for-Obeticholic-Acid-for-the-Treatment-of-Fibrosis-Due-to-NASH.html.
8. Cheng AL, Hsu C, Chan SL, Choo SP, Kudo K. Challenges of combination therapy with immune checkpoint inhibitors for hepatocellular carcinoma. *J Hepatol* 2020;**72**:307−19.
9. Kadowaki T, Yamauchi T. Adiponectin and adiponectin receptors. *Endocr Rev* 2005;**26**:439−51.
10. Kita S, Maeda N, Shimomura I. Interorgan communication by exosomes, adipose tissue, and adiponectin in metabolic syndrome. *J Clin Invest* 2019;**129**:4041−9.
11. Havel PJ. Update on adipocyte hormones: regulation of energy balance and carbohydrate/lipid metabolism. *Diabetes* 2004;**53**:S143−51.
12. Zhao C, Wu M, Zeng N, Xiong M, Hu W, Lv W, et al. Cancer-associated adipocytes: emerging supporters in breast cancer. *J Exp Clin Cancer Res* 2020;**39**:156.
13. Yamamoto J, Yamane T, Oishi Y, Shimizu M, Tadaishi M, Kobayashi-Hattori K. Chrysanthemum promotes adipocyte differentiation, adiponectin secretion and glucose uptake. *Am J Chin Med* 2015;**43**:255−67.
14. Fujishima Y, Maeda N, Matsuda K, Masuda S, Mori T, Fukuda S, et al. Adiponectin association with T-cadherin protects against neointima proliferation and atherosclerosis. *Faseb J* 2017;**31**:1571−83.
15. Chung SJ, Nagaraju GP, Nagalingam A, Muniraj N, Kuppusamy P, Walker A, et al. ADIPOQ/adiponectin induces cytotoxic autophagy in breast cancer cells through STK11/LKB1-mediated activation of the AMPK−ULK1 axis. *Autophagy* 2017;**13**:1386−403.
16. Kumar P, Raeman R, Chopyk DM, Smith T, Verma K, Liu Y, et al. Adiponectin inhibits hepatic stellate cell activation by targeting the PTEN/AKT pathway. *Biochim Biophys Acta, Mol Basis Dis* 2018;**1864**:3537−45.
17. Tardelli M, Claudel T, Bruschi FV, Moreno-Viedma V, Trauner M. Adiponectin regulates AQP3 *via* PPARalpha in human hepatic stellate cells. *Biochem Biophys Res Commun* 2017;**490**:51−4.
18. Bugianesi E, Pagotto U, Manini R, Vanni E, Gastaldelli A, de Iasio R, et al. Plasma adiponectin in nonalcoholic fatty liver is related to hepatic insulin resistance and hepatic fat content, not to liver disease severity. *J Clin Endocrinol Metab* 2005;**90**:3498−504.
19. Musso G, Gambino R, Durazzo M, Biroli G, Carello M, Fagà E, et al. Adipokines in NASH: postprandial lipid metabolism as a link between adiponectin and liver disease. *Hepatology* 2005;**42**:1175−83.
20. Alzahrani B, Iseli T, Ramezani-Moghadam M, Ho V, Wankell M, Sun EJ, et al. The role of AdipoR1 and AdipoR2 in liver fibrosis. *Biochim Biophys Acta, Mol Basis Dis* 2018;**1864**:700−8.
21. Wang H, Zhang H, Zhang Z, Huang B, Cheng X, Wang D, et al. Adiponectin-derived active peptide ADP355 exerts anti-inflammatory and anti-fibrotic activities in thioacetamide-induced liver injury. *Sci Rep* 2016;**18**:19445.
22. Ma L, Zhang Z, Xue X, Wan Y, Ye B, Lin K. A potent peptide as adiponectin receptor 1 agonist to against fibrosis. *J Enzym Inhib Med Chem* 2017;**32**:624−31.
23. Xu H, Zhao Q, Song N, Yan Z, Lin R, Wu S, et al. AdipoR1/-AdipoR2 dual agonist recovers nonalcoholic steatohepatitis and related fibrosis *via* endoplasmic reticulum−mitochondria axis. *Nat Commun* 2020;**11**:5807.
24. Duca L, Blanchevoye C, Cantarelli B, Ghoneim C, Dedieu S, Delacoux F, et al. The elastin receptor complex transduces signals through the catalytic activity of its Neu-1 subunit. *J Biol Chem* 2007;**282**:12484−91.
25. Scandolera A, Odoul L, Salesse S, Guillot A, Blaise S, Kawecki C, et al. The elastin receptor complex: a unique matricellular receptor with high anti-tumoral potential. *Front Pharmacol* 2016;**7**:32.
26. Siemianowicz K, Likus W, Francuz T, Garczorz W. Effect of elastin-derived peptides on the production of tissue inhibitor of metalloproteinase-1, -2, and -3 and the ratios in various endothelial cell lines. *Exp Ther Med* 2015;**9**:2245−50.
27. Romier B, Ivaldi C, Sartelet H, Heinz A, Schmelzer CEH, Garnotel R, et al. Production of elastin-derived peptides contributes to the development of nonalcoholic steatohepatitis. *Diabetes* 2018;**67**:1604−15.
28. Robinet A, Millart H, Oszust F, Hornebeck W, Bellon G. Binding of elastin peptides to S-Gal protects the heart against

ischemia/reperfusion injury by triggering the RISK pathway. *FASEB J* 2007;**21**:1968−78.

29. He B, Lu C, Zheng G, He X, Wang M, Chen G, et al. Combination therapeutics in complex diseases. *J Cell Mol Med* 2016;**20**:2231−40.

30. Santhekadur PK, Kumar DP, Sanyal AJ. Preclinical models of non-alcoholic fatty liver disease. *J Hepatol* 2018;**68**:230−7.

31. Van Herck MA, Vonghia L, Francque SM. Animal models of nonalcoholic fatty liver disease-a starter's guide. *Nutrients* 2017;**9**:1072.

32. Seglen PO. Preparation of isolated rat liver cells. *Methods Cell Biol* 1976;**13**:29−83.

33. Vuppalanchi R, Marri S, Kolwankar D, Considine RV, Chalasani N. Is adiponectin involved in the pathogenesis of nonalcoholic steatohepatitis? A preliminary human study. *J Clin Gastroenterol* 2005;**39**:237−42.

34. Moravcová A, Červinková Z, Kučera O, Mezera V, Rychtrmoc D, Lotková H. The effect of oleic and palmitic acid on induction of steatosis and cytotoxicity on rat hepatocytes in primary culture. *Physiol Res* 2015;**64**:S627−36.

35. Nasrallah CM, Horvath TL. Mitochondrial dynamics in the central regulation of metabolism. *Nat Rev Endocrinol* 2014;**10**:650−8.

36. Palikaras K, Lionaki E, Tavernarakis N. Mechanisms of mitophagy in cellular homeostasis, physiology and pathology. *Nat Cell Biol* 2018; **20**:1013−22.

37. Palikaras K, Daskalaki I, Markaki M, Tavernarakis N. Mitophagy and age-related pathologies: development of new therapeutics by targeting mitochondrial turnover. *Pharmacol Ther* 2017;**178**:157−74.

38. Snezhkina AV, Kudryavtseva AV, Kardymon OL, Savvateeva MV, Melnikova NV, Krasnov GS, et al. ROS generation and antioxidant defense systems in normal and malignant cells. *Oxid Med Cell Longev* 2019;**2019**:6175804.

39. Scherz-Shouval R, Elazar Z. Regulation of autophagy by ROS: physiology and pathology. *Trends Biochem Sci* 2011;**36**:30−8.

40. Maycotte P, Aryal S, Cummings CT, Thorburn J, Morgan MJ, Thorburn A. Chloroquine sensitizes breast cancer cells to chemotherapy independent of autophagy. *Autophagy* 2012;**8**:200−12.

41. Eng KE, Panas MD, Karlsson Hedestam GB, McInerney GM. A novel quantitative flow cytometry-based assay for autophagy. *Autophagy* 2010;**6**:634−41.

42. Zhao X, Kwan JYY, Yip K, Liu PP, Liu FF. Targeting metabolic dysregulation for fibrosis therapy. *Nat Rev Drug Discov* 2020;**19**: 57−75.

43. Rockey DC, Bell PD, Hill JA. Fibrosis—a common pathway to organ injury and failure. *N Engl J Med* 2015;**372**:1138−49.

44. Dasarathy S. Is the adiponectin-AMPK-mitochondrial axis involved in progression of nonalcoholic fatty liver disease?. *Hepatology* 2014;**60**:22−5.

45. Izdebska M, Piatkowska-Chmiel I, Korolczuk A, Herbet M, Gawronska-Grzywacz M, Gieroba R, et al. The beneficial effects of resveratrol on steatosis and mitochondrial oxidative stress in HepG2 cells. *Can J Physiol Pharmacol* 2017;**95**:1442−53.

46. Handa P, Maliken BD, Nelson JE, Morgan-Stevenson V, Messner DJ, Dhillon BK, et al. Reduced adiponectin signaling due to weight gain results in nonalcoholic steatohepatitis through impaired mitochondrial biogenesis. *Hepatology* 2014;**60**:133−45.

47. van der Vaart JI, Boon MR, Houtkooper RH. The role of AMPK signaling in brown adipose tissue activation. *Cells* 2021;**10**:1122.

48. Garcia D, Shaw RJ. AMPK: mechanisms of cellular energy sensing and restoration of metabolic balance. *Mol Cell* 2017;**66**: 789−800.

49. Herzig S, Shaw RJ. AMPK: guardian of metabolism and mitochondrial homeostasis. *Nat Rev Mol Cell Biol* 2018;**19**:121−35.

50. Pickles S, Vigié P, Youle RJ. Mitophagy and quality control mechanisms in mitochondrial maintenance. *Curr Biol* 2018;**28**:R170−85.